AGU PUBLICATIONS

Earth's Future

Supporting Information for

Identifying Coherence Across End-of-Century Montane Snow Projections in the Western United States

Justin M. Pflug[1,2], Sujay V. Kumar[1], Ben Livneh[3], Ethan D. Gutmann[4], Sudershan Gangrade[5,6], Shih-Chieh Kao[5,6]

[1]Hydrological Sciences Laboratory, NASA Goddard Space Flight Center, Greenbelt, Maryland
[2]Earth System Sciences Interdisciplinary Center, University of Maryland, College Park, College Park, Maryland
[3]Cooperative Institute for Research in Environmental Sciences, University of Colorado, Boulder, Boulder, Colorado
[4]National Center for Atmospheric Research, Boulder, Colorado
[5]Environmental Sciences Division, Oak Ridge National Laboratory, Oak Ridge, Tennessee
[6]Climate Change Science Institute, Oak Ridge National Laboratory, Oak Ridge, Tennessee

Contents of this file

Introduction

Text S1 and Text S2 provide additional details on the snow projection datasets compared in the main text. Figures S1 through S12 provide additional figures in formats analogous to those presented in the main text, but for different domains and periods. Finally Table 1 includes snow projection statistics, including specific statistics and values referenced in the main text. Here, these text, figures, and statistics support and complement the findings of the associated study, but are not necessary for the understanding of the study results presented in the main text.

Text S1: NEX6-C and NEX6-M modeling procedure

The NEX6-M and NEX6-C snow water equivalent (SWE) projections developed for this study were made using a two-step modeling approach, which 1) developed baseline simulations representative of snow evolution in historical periods, and 2) perturbed the baseline simulations with future climate-change signals. While straightforward, this change-factor approach (also termed the *delta method*) is a reliable approach for determining hydrological and ecological climate sensitivities (Barsugli et al., 2020; McKelvey et al., 2011; Sofaer et al., 2017).

Historical snow simulations were forced with meteorological data from the Modern-Era Retrospective Reanalysis, version 2 (MERRA-2; Gelaro et al., 2017). The forcing variables used were air temperature, specific humidity, downwelling shortwave radiation, downwelling longwave radiation, wind speed, wind direction, surface pressure, and precipitation. Prior to forcing simulations, MERRA-2 was downscaled to the model resolution (0.01°). Coarse grid cell mean precipitation from MERRA-2 was spatially disaggregated using the underlying and finer-scale (1 km) monthly climatology precipitation patterns from Parameter-elevation Regressions on Independent Slopes Model (PRISM; Daly et al., 2008, 1997). MERIT elevations maps and terrain-based lapse rates (e.g., Cosgrove et al., 2003) were also used to downscale meteorological forcing data. Finally, slope and aspect corrections were used to calculate terrain shading impacts. The downscaling approaches used here are discussed in-depth in Arsenault et al. (2018).

Future climate change signals were derived from the Coupled Model Intercomparison Project, phase 6 (CMIP6; Eyring et al., 2016). Prior to accessing this data, CMIP6 daily-average historical and future climate data were downscaled to 0.1° resolution by the NASA Earth Exchange Global Daily Downscaled Projections (NEX-GDD-CMIP6; Thrasher et al., 2022). NEX-GDDP-CMIP6 data was downscaled using the popular bias correction spatial disaggregation (BCSD) approach (Wood et al., 2004), which uses overlapping periods of climate models (from CMIP6) and historical observations as the basis for determining the climate model bias and sub-grid variability at monthly intervals. Here, observations came from the reanalysis-based Global Meteorological Forcing Dataset (GMFD; Sheffield et al., 2006). Readers are referenced to Thrasher et al. (2022) and Wood et al. (2004) for more information on NEX-GDDP-CMIP6 and BCSD, respectively.

The Land Information System (LIS; Kumar et al., 2006) was used to simulate snow evolution at fine spatial resolutions (0.01°, ~1 km) and hourly timesteps over the five Western US montane watersheds. LIS simulations in this study were performed using the Noah-Multiparameterization (Noah-MP) land surface model (Niu et al., 2011), which accounts for a discrete canopy layer, and multilayer snow representations. Landcover classifications came from satellite-derived International Geosphere-Biosphere

Programme (IGBP) classifications (Friedl et al., 2022, 2002), and soil maps were derived from the International Soil Reference and Information Centre (ISRIC; Batjes, 1995). Spatially varying maximum snow albedo was prescribed using historic observations (Barlage et al., 2005) from the MODerate Resolution Imaging Spectroradiometer (MODIS). Finally, modeled snow albedo decayed in accordance to a decay factor from the Canadian Land Surface Scheme (CLASS) parameterization (Verseghy, 1991). Snowfall and rainfall were partitioned at each hourly timestep using a method from Jordan (1991),

$$\begin{array}{ll} F_{snow} = 1: & T_{air} < 0.5°C \\ F_{snow} = 1 - [0.2T_{air}]: & 0.5°C < T_{air} < 2.0°C \\ F_{snow} = 0.6: & 2.0°C < T_{air} \leq 2.5°C \\ F_{snow} = 0: & T_{air} > 2.5°C \end{array}$$

where T_{air} is hourly and 0.01° air temperature and F_{snow} is the fraction of precipitation that fell as snow. This model setup is similar to a number of recent studies that employed LIS and Noah-MP for snow modeling purposes (Cho et al., 2022; Kim et al., 2021; Wrzesien et al., 2022).

We partitioned the historical and future records into discrete records of time that were long enough to encompass climate variability, while short enough to compare climate impacts on snow across multiple periods between present-day and 2100. Here, we used a variogram-type approach to determine the number of years at which historical and projected interannual climate variability plateaued (e.g., Chiverton et al., 2015; Subyani, 2019). First, we calculated the downscaled NEX-GDDP-CMIP6 median air temperature for each 0.01° grid cell across all days in a random water-year. Then, the spatial coefficient of variation (standard deviation divided by the mean) was calculated. This was performed initially for one year, and then was repeated, starting again in the same year, but including successively longer periods of time (e.g., 1 year, 2 years, 3 years, and so on). By plotting the air temperature coefficient of variation versus the number of years it was calculated over, we could determine the number of years beyond which interannual climate variability did not increase further (i.e., the variogram reaches a plateau). This approach was repeated for both air temperature and cumulative precipitation, and for randomly selected starting years.

In all cases, periods of 14 – 18 years minimized the impact of annual climate variability on median air temperature and precipitation. Here, to increase the likelihood of encompassing interannual climate variability, we partitioned the historical and future climate records into 20-year windows. Since the NEX-GDDP-CMIP6 "historic" data record runs from January 1950 to December 2014, the 20-year historical period for this study was assumed to span from water-year 1995 to water-year 2014 (October 1994 to September 2014). Since the CMIP6 "projections" started on January 2015, we selected the first 20-year future period to span between October 2015 and September 2035 (water-year 2016 to 2035). We then identified three more future 20-year periods including water-years: 2036 – 2055, 2056 – 2075, and 2076 – 2095. The 20-year windows used in this study align with period-lengths used by several other climate studies (e.g., Mahony et al., 2022; Planton et al., 2012; Reifen and Toumi, 2009).

Baseline snow simulations were developed to represent historical snow evolution between water-year 1995 and 2014. For each individual grid cell and hour of the water-year, model forcings were provided from the downscaled MERRA-2 forcing discussed above. We then used a two-step calibration approach to match 1995 – 2014 total snow volume from the Western US reanalysis (Fang et al., 2020; Margulis et al., 2016) (see Section 2.1 in the main text). Since precipitation is commonly cited as the first-order driver of model errors in mountainous regions (e.g., Cho et al., 2022; Günther et al., 2019; Raleigh et al., 2015; Wayand et al., 2013; Wrzesien et al., 2022), we first focused on tuning the precipitation forcing. Starting in October of each year, the simulated cumulative increases in SWE were calculated from LIS simulations. This was then compared to the cumulative increases SWE from the WUS reanalysis in the same month. Using the percent-difference between the end-of-month cumulative increases in SWE from the reanalysis and LIS simulation, cumulative precipitation for the baseline simulation was scaled (assumed to be constant in space). Snow simulations were then performed again, and this procedure was repeated until end-of-month cumulative increases in SWE from the reanalysis and LIS-simulations converged. This method was repeated for each successive month in the snow accumulation season, between October and May.

Overall, the baseline simulation tended to have SWE that was more spatially homogeneous than the snow reanalysis. This is a known issue for land surface models in mountainous terrain, which do not always represent complex processes like wind-redistribution, preferential deposition, and avalanching. While modeling approaches have been developed to correct for these issues (e.g., Pflug et al., 2021; Vögeli et al., 2016; Wrzesien et al., 2022), it was not clear whether spatial disagreements in SWE between the baseline simulation and reanalysis were due to missing processes in Noah-MP, or issues with the spatial heterogeneity of model forcing (Livneh et al., 2014). To avoid over-fitting the baseline simulations, we only calibrated the precipitation using the approach discussed above. We expect this simulation to serve as a strong baseline for historical snow evolution, especially given the first-order elevation, vegetation, and terrain-shading drivers of snow accumulation and depletion represented in the LIS modeling framework. In fact, after calibration, the total snow volume for these two datasets had a temporal coefficient of variation of greater than 0.95, and the SWE spatial coefficient of variation at peak snowpack timing ranged between 0.78 and 0.91, across the five domains.

The NEX-GDDP-CMIP6 product was used to derive 20-year average changes (relative to the historical period) to meteorological conditions for each model grid cell. These change signals were calculated for a set of 23 Global Climate Models (GCMs) available at the time of this project (Thrasher et al., 2022) and emissions scenarios from Shared Socioeconomic Pathway 2-4.5 (SSP 2-4.5). The GCMs used in this study can be found in Text S2. For each GCM, model grid cell, and day of the water year, the difference between the median future (e.g., 2056 – 2075) and historical (1995 – 2016) climate variables were calculated. Climate conditions for a single day of the water year can vary significantly across 20-year time frames, so we do not expect change factors calculated at daily time steps to be representative of the underlying trends with climate change. Therefore, following approaches used by Barsugli et al. (2020), the difference between future and historical climate variables were averaged across monthly time frames to calculate change-factors, or future differences to the monthly-average air temperature, relative humidity, shortwave radiation, longwave radiation, wind speed, and cumulative precipitation, relative to the historical period. We noted that differences in climate variables at monthly time frames sometimes resulted in sporadic change-factors. For example, at monthly intervals, a difference of one or two precipitation events could result in significant differences (-100% to 150%) in monthly cumulative precipitation. To minimize this issue, we aggregated monthly change-factors across three-month moving windows, including the months both before and after the focus month. These change signals were then applied to the baseline simulation to generate the two novel snow projections presented in the main text. We did this two ways:

1. **NEX6-C:** NEX-GDDP-CMIP6 20-year average monthly projected changes to climate were applied to the 20-year baseline calibrated simulation. Despite the interannual variations in meteorological and snow conditions, the monthly perturbations to the climate variables were assumed to be the same in each year.
2. **NEX6-M:** The same climate perturbations as the NEX6-C simulation were used to perturb the snow simulation. However, these perturbations were applied to a single-year baseline simulation performed using the 20-year median meteorological conditions from the historical period (1995 – 2014).

Text S2: GCMs used by each snow projection dataset

NEX6-M [CMIP6, SSP2-4.5]: ACCESS-CM2, ACCESS-ESM1-5, CESM2, CESM2-WACCM, CMCC-ESM2, CNRM-CM6-1, CNRM-ESM2-1, EC-Earth3, FGOALS-g3, GFDL-CM4, GFDL-CM4_gr2, GFDL-ESM4, GISS-E2-1-G, ITM-ESM, INM-CM4-8, INM-CM5-0, KACE-1-0-G, MIROC-ES2L, MPI-ESM1-2-HR, MP1-EMS1-2-LR, MRI-ESM2-0, NorESM2-LM, NorESM2-MM

NEX6-C [CMIP6, SSP2-4.5]: ACCESS-CM2, ACCESS-ESM1-5, CESM2, CESM2-WACCM, CMCC-ESM2, CNRM-CM6-1, CNRM-ESM2-1, EC-Earth3, FGOALS-g3, GFDL-CM4, GFDL-CM4_gr2, GFDL-ESM4, GISS-E2-1-G, ITM-ESM, INM-CM4-8, INM-CM5-0, KACE-1-0-G, MIROC-ES2L, MPI-ESM1-2-HR, MP1-EMS1-2-LR, MRI-ESM2-0, NorESM2-LM, NorESM2-MM

LOCA5 [CMIP5, RCP 4.5]: ACCESS1-0, ACCESS1-3, CESM1-BGC, CESM1-CAM5, CMCC-CM, CMCC-CMS, CNRM-CM5,EC-Earth, FGOALS-g2, GFDL-CM3, GFDL-EMS2G, GFDL-EMS2M, GISS-E2-H, GISS-E2-R, INMCM4, MIROC-ESM, MIROC-ESM-CHEM, MIROC5, MPI-ESM-LR, MPI-ESM-MR, MRI-CGCM3, NorESM1-M

BCSD5 [CMIP5, RCP 4.5]: ACCESS1-0, BCC-CSM1-1, BCC-CSM1-1-M, CANESM2, CCSM4, CESM1-BGC, CESM1-CAM5, CMCC-CM, CNRM-CM5, CSIRO-Mk3-6-0, FGOALS-G2, FIO-ESM, GFDL-CM3, GFDL-EMS2G, GFDL-EMS2M, GISS-E2-H-CC, GISS-E2-R, GISS-E2-R-CC, HadGEM2-AO, HadGEM2-CC, HadGEM2-ES, INMCM4, IPSL-CM5A-MR, IPSL-CM5B-LR, MIROC-ESM, MIROC-ESM-CHEM, MIROC5, MPI-ESM-LR, MPI-ESM-MR, MRI-CGCM3, NorESM1-M

MACA5 [CMIP5, RCP 4.5]: BCC-CSM1-1-M, CANESM2, CCSM4, CNRM-CM5, CSIRO-Mk3-6-0, HadGEM2-CC, HadGEM2-ES, IPSL-CM5A-MR, MIROC5, NorESM1-M

DBCCA6 [CMIP6, SSP2-4.5]: ACCES-CM2, BCC-CSM2-MR, CNRM-ESM2-1, MPI-ESM1-2-HR, MRI-ESM2-0, NorESM2-MM

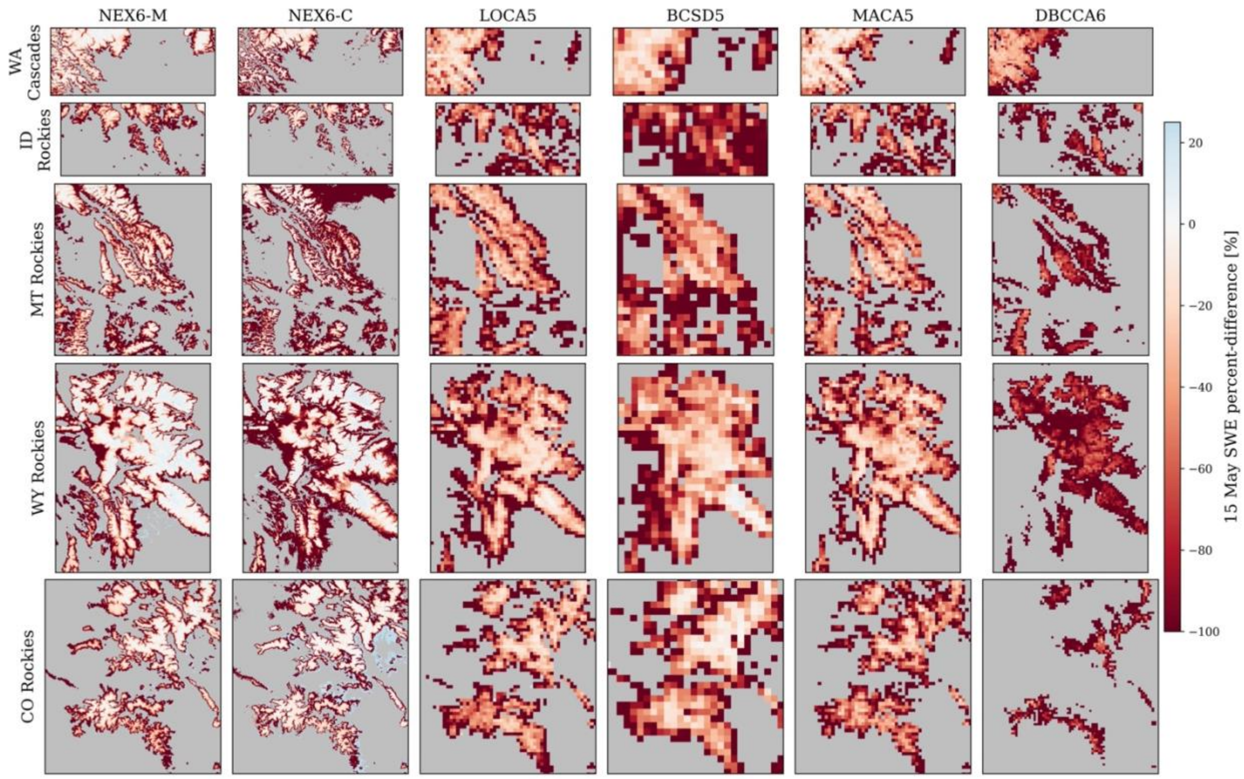

Figure S1. Spatial plots of GCM-ensemble median percent changes to 15 May SWE.

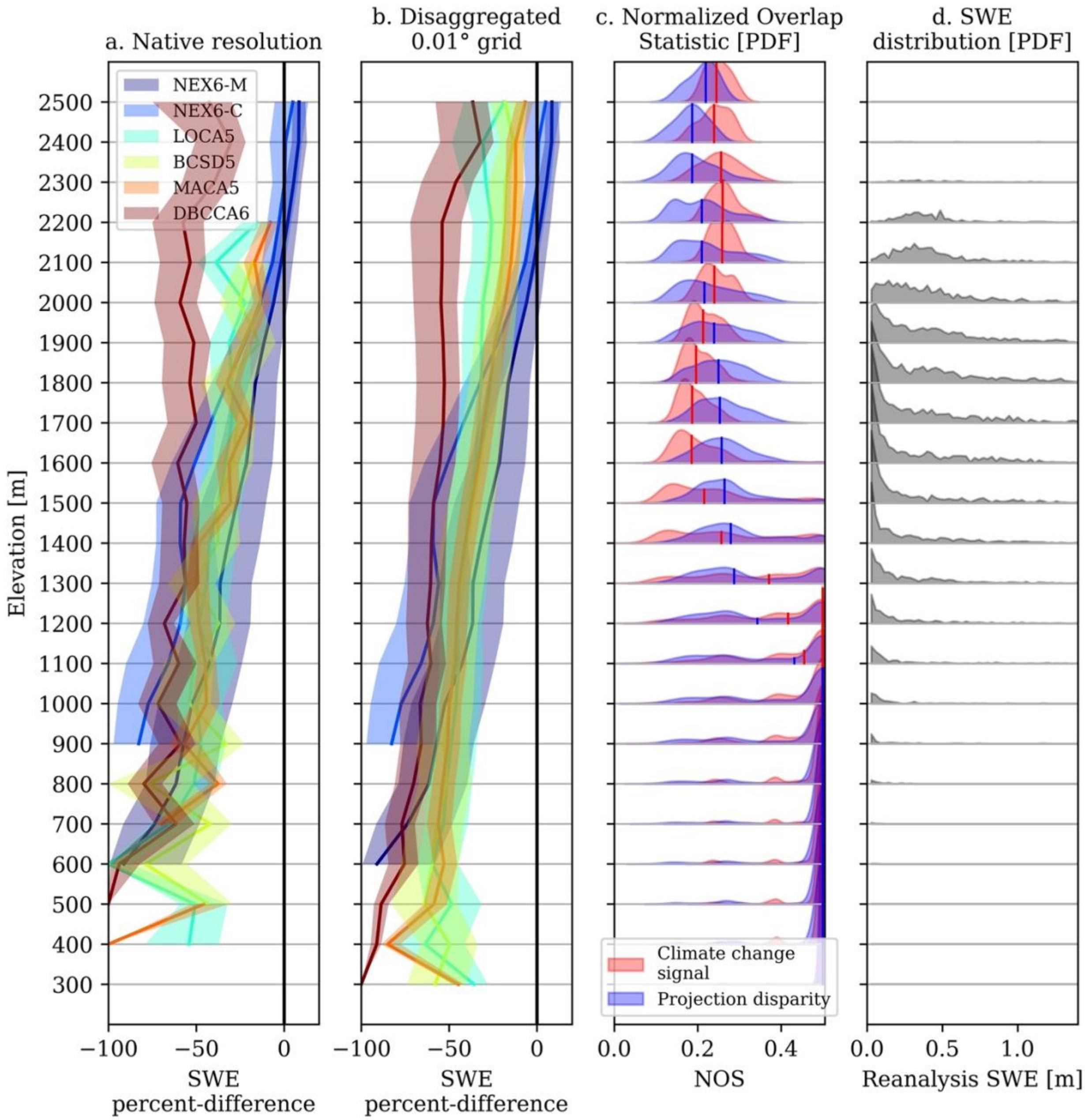

211
212 Figure S2. Same as Figure 5, but shows data for the WA Cascades domain on 15 May.

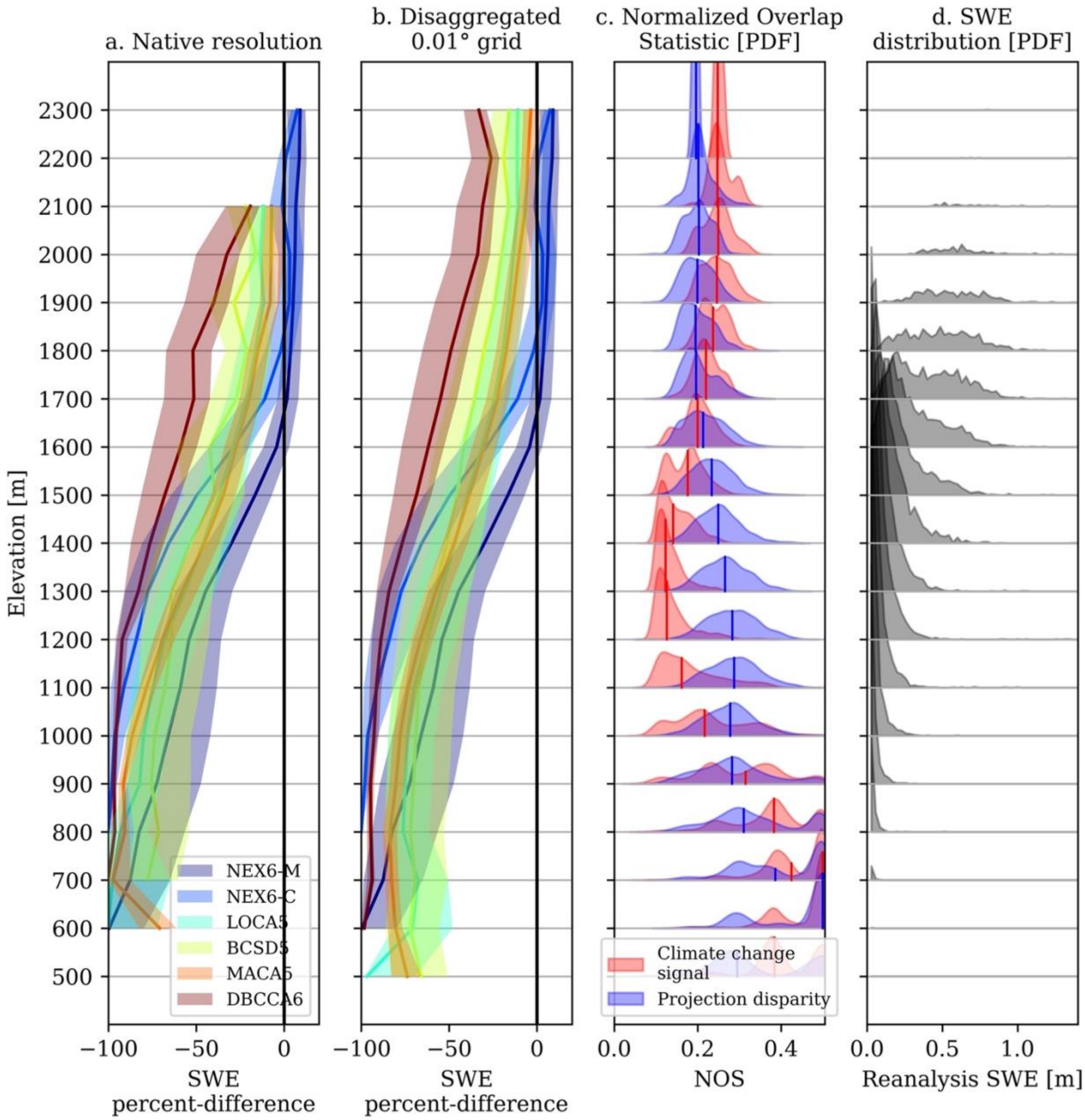

Figure S3. Same as Figure 5, but shows data for the ID Rockies domain on 15 April.

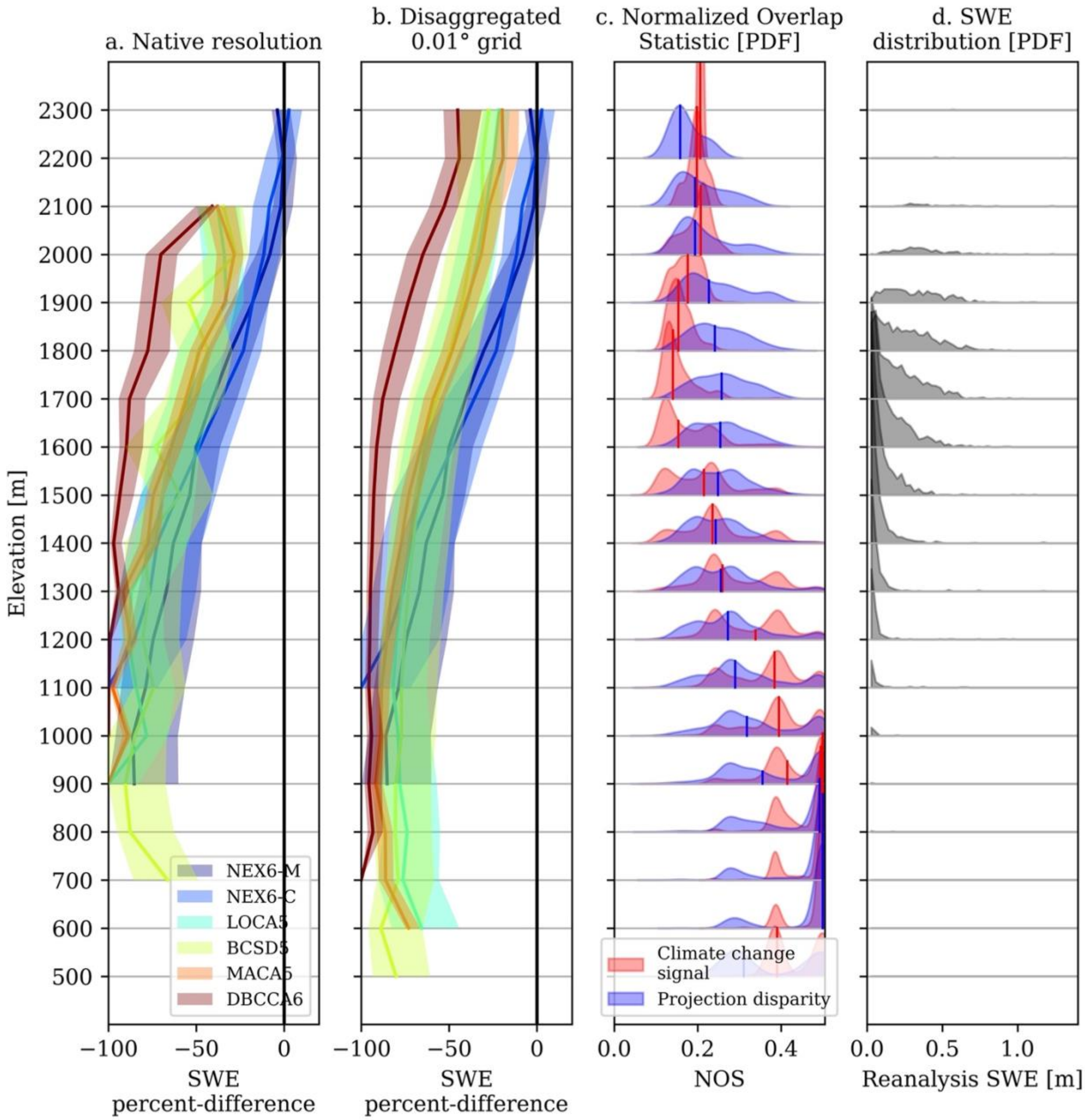

215
216 Figure S4. Same as Figure 5, but shows data for the ID Rockies domain on 15 May.

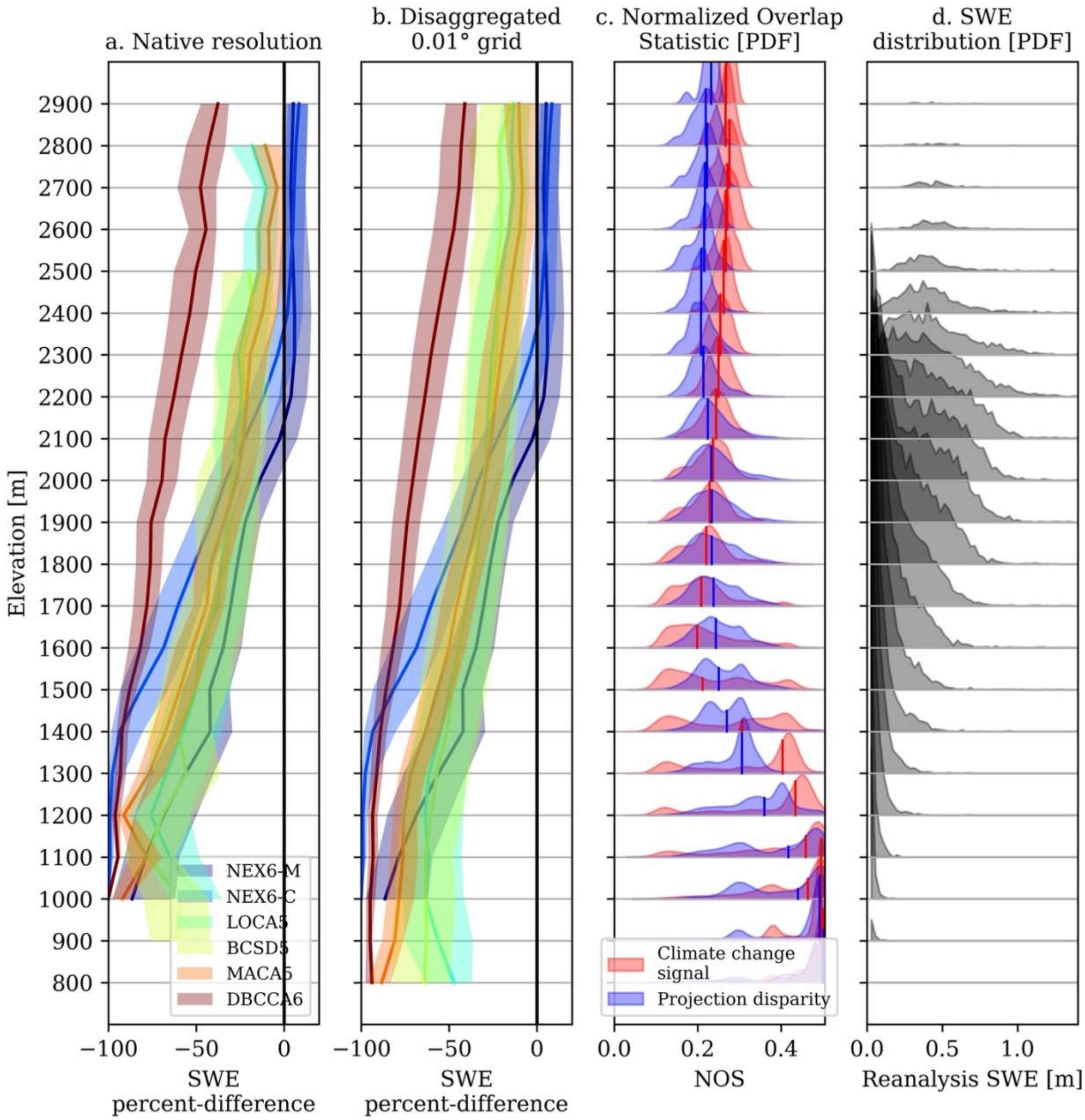

217
218 Figure S5. Same as Figure 5, but shows data for the MT Rockies domain on 15 April.

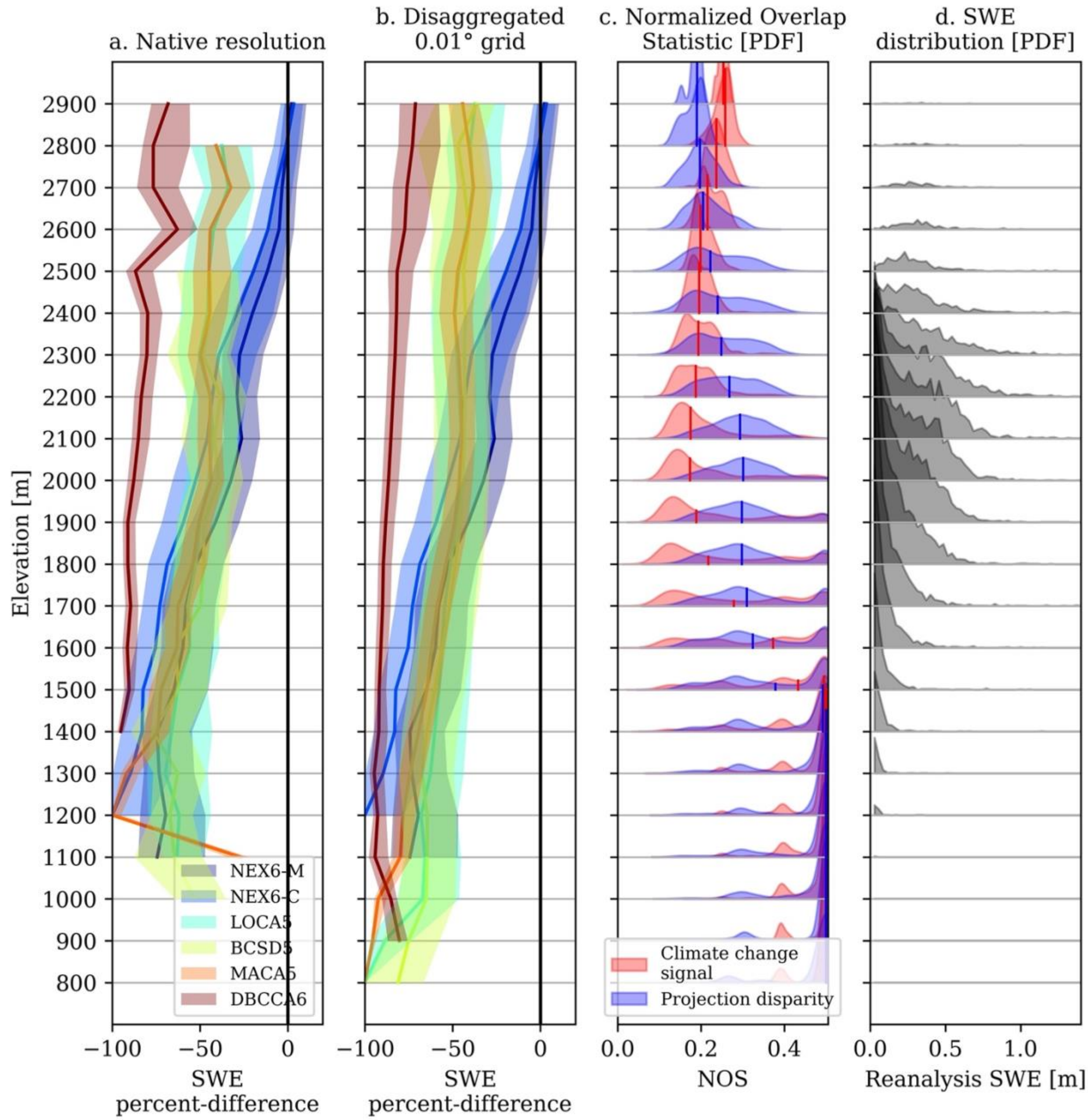

219
220 Figure S6. Same as Figure 5, but shows data for the MT Rockies domain on 15 May.

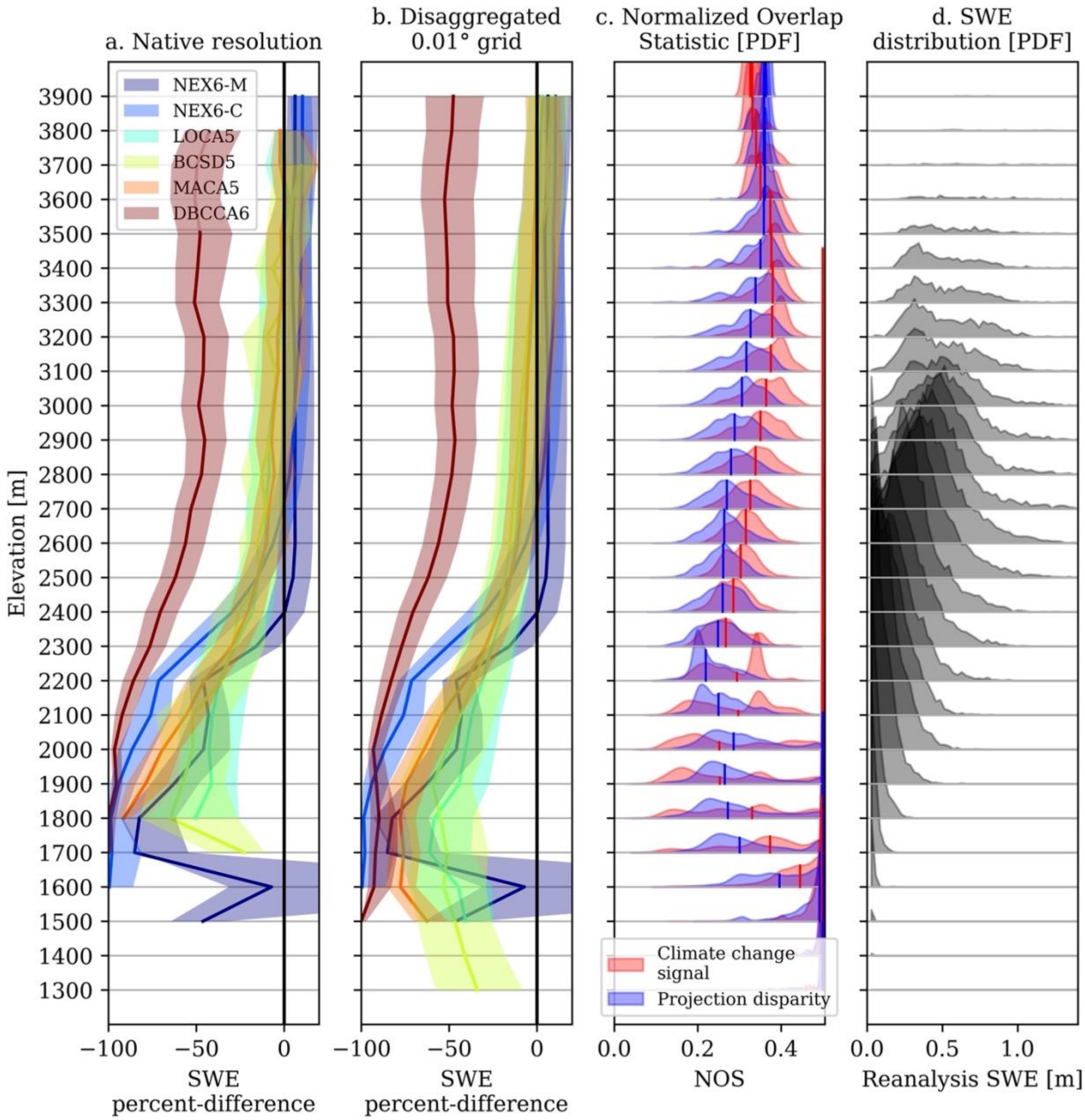

221
222 Figure S7. Same as Figure 5, but shows data for the WY Rockies domain on 15 April.

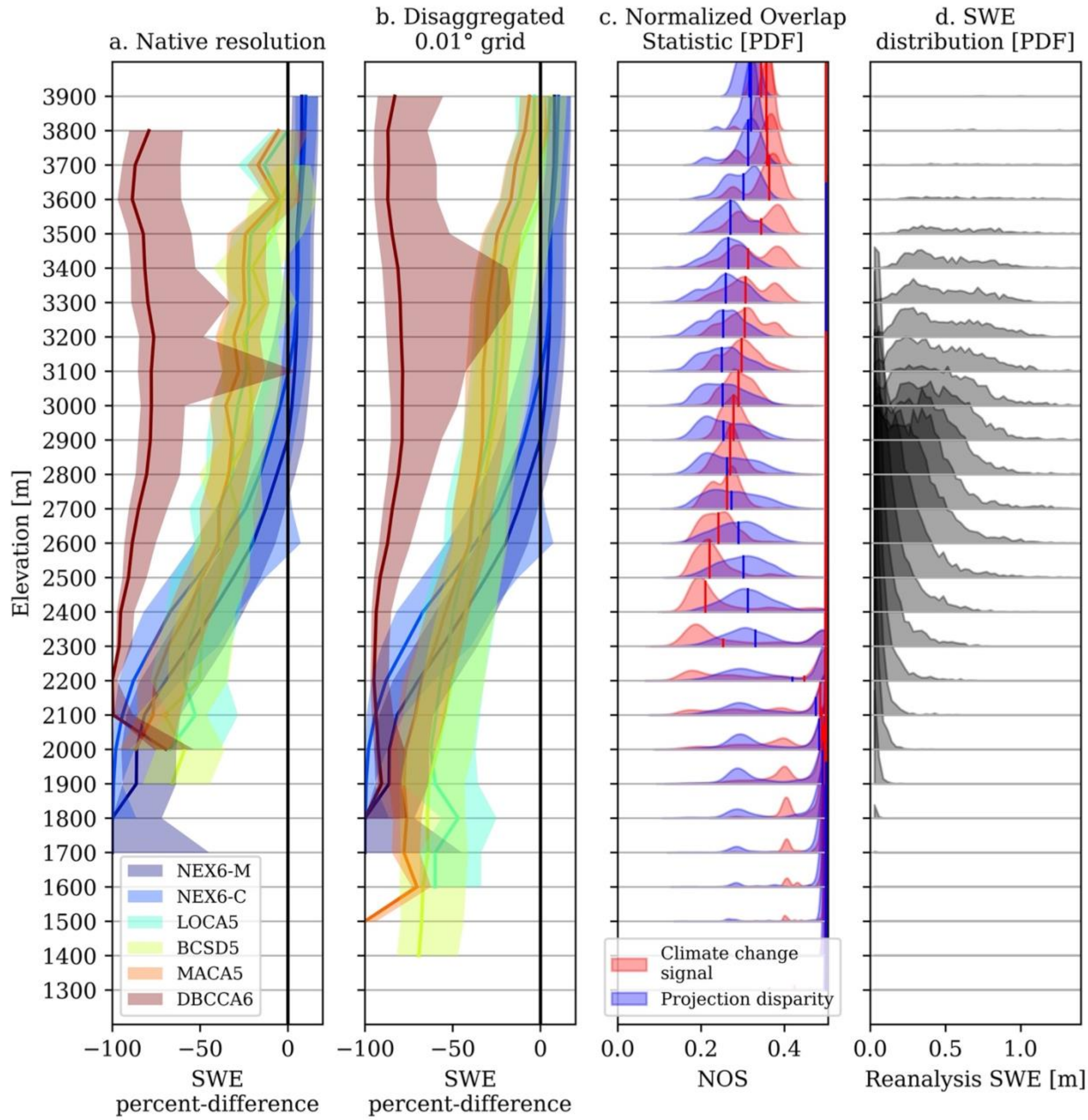

Figure S8. Same as Figure 5, but shows data for the WY Rockies domain on 15 May.

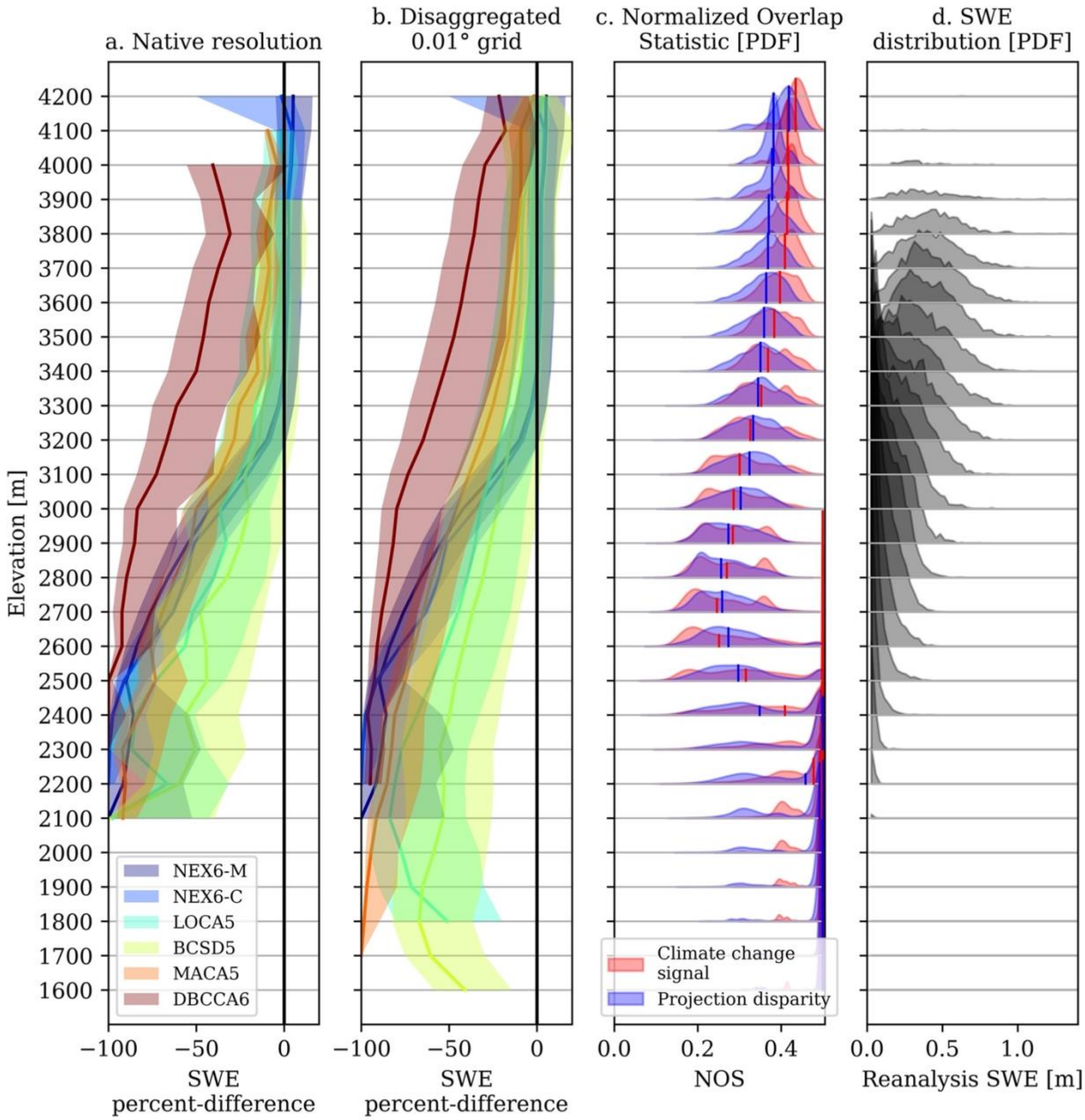

Figure S9. Same as Figure 5, but shows data for the CO Rockies domain on 15 April.

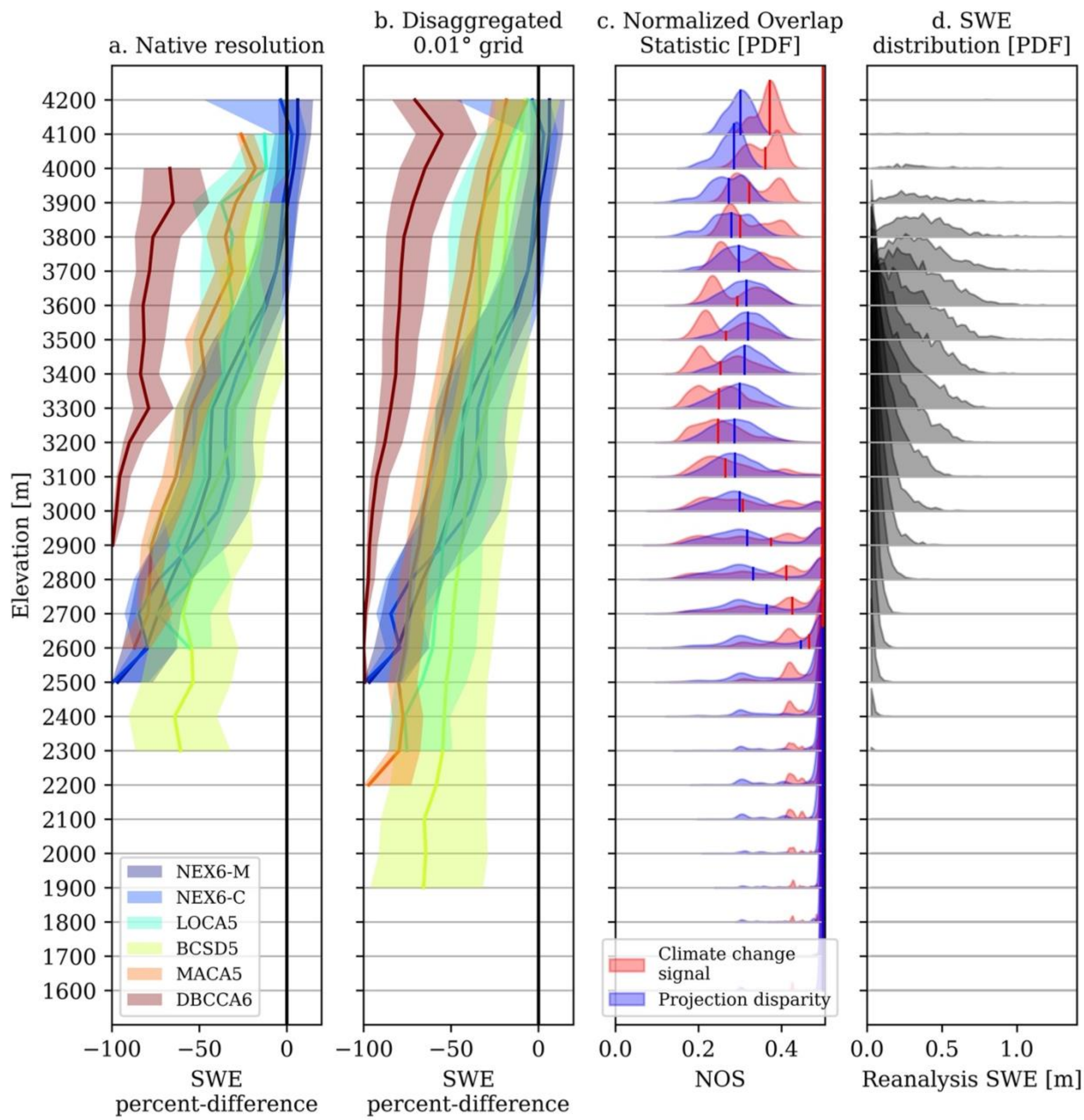

227
228 Figure S10. Same as Figure 5, but shows data for the CO Rockies domain on 15 May.

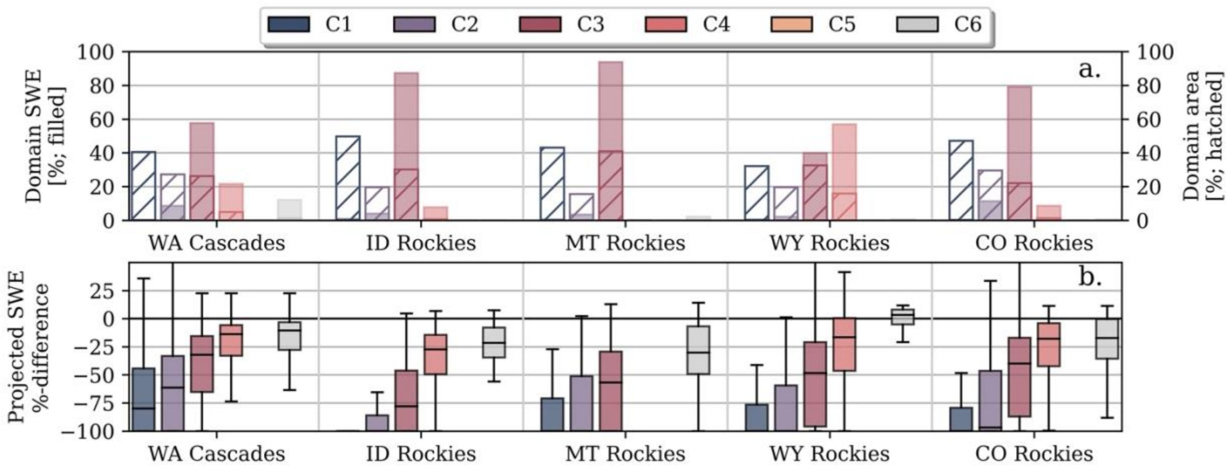

Figure S11. Same as Figure 8, but shows data for 15 May.

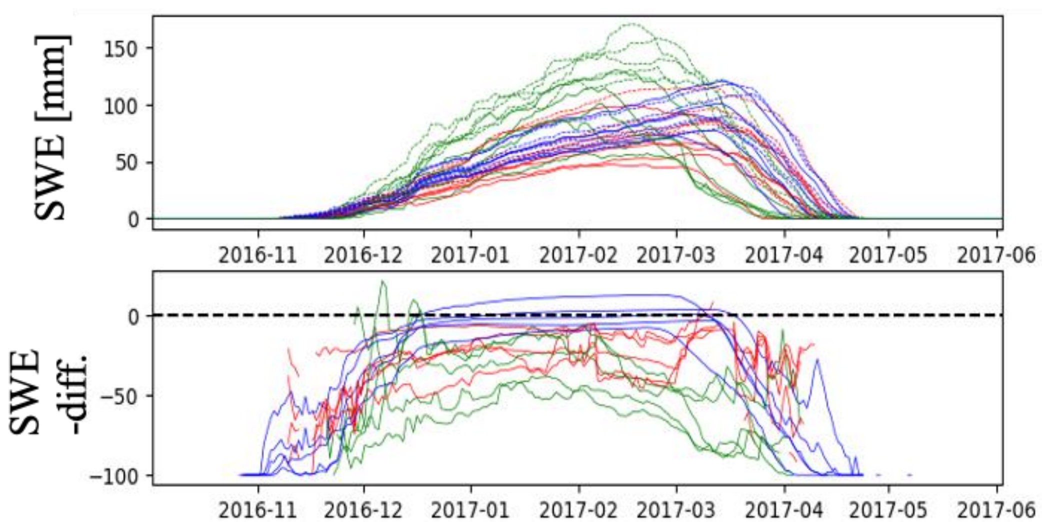

Figure S12. SWE magnitude (top) in the WA Cascades domain averaged for 4 different elevation bands in the early 21st century (solid) and end-of-century (dashed periods). The lines are colored by the data from NEX6-M (blue), NEX6-C (red), and DBCCA6 (green) proejctions. The bottom plot depicts the percent-difference between the end-of-century and early 21st century SWE from each day presented in the top plot.

Table S1. Snow projection statistics. Statistics are broken down by elevation bands selected to highlight spans where different elevational patterns emerge for each projection dataset.

Domain	**Projection**	**Maximum elevation resolved**	**First elevation with SWE increases**	**Lower limit**	**Upper limit**	**Mean SWE %-difference**	**SWE projection gradient [SWE %-diff/100m]**
WA Cascades	NEX6-M	2775	1650	450	1350	-68	2
				1350	1650	-11	12
				1650	2550	5	0
	NEX6-C	2775	1950	550	1350	-88	3
				1350	1850	-24	12
				1850	2550	1	0
	LOCA5	2434	-	350	2250	-47	3
	BCSD5	2124	-	250	1850	-57	4
	MACA5	2434	2050	350	1450	-64	2
				1450	2250	-10	4
	DBCCA6	2463	-	350	2550	-52	2
ID Rockies	NEX6-M	2295	1750	550	1350	-79	6
				1350	1650	-19	12
				1650	2350	3	1
	NEX6-C	2295	1850	750	1350	-94	4
				1350	1850	-41	18
				1850	2350	2	0
	LOCA5	2076	-	550	2150	-61	5
	BCSD5	2103	-	650	2150	-65	4
	MACA5	2076	-	550	850	-94	-3
				850	2150	-57	6
	DBCCA6	2105	-	650	2150	-79	4
MT Rockies	NEX6-M	2967	2150	950	1850	-64	6
				1850	2150	-14	6
				2150	2950	4	0
	NEX6-C	2967	2450	950	1450	-98	4
				1450	2350	-48	9
				2350	2950	3	1
	LOCA5	2813	-	950	2850	-52	2
	BCSD5	2801	-	850	2550	-54	3
	MACA5	2813	-	950	2850	-49	4
	DBCCA6	2868	-	950	2950	-79	1
WY	NEX6-M	3916	2450	1450	2250	-68	7

				2250	2450	-8	15
				2450	3950	5	0
	NEX6-C	3916	2750	1550	2250	-88	8
				2250	2450	-40	19
				2450	3950	-1	2
	LOCA5	3793	3550	1750	2450	-55	6
				2450	3850	-12	1
	BCSD5	3691	3450	1650	2550	-49	7
				2550	3750	-11	1
	MACA5	3793	3850	1750	2550	-48	9
				2550	3850	-8	1
	DBCCA6	3830	-	1650	2750	-77	5
				2750	3850	-52	0
CO Rockies	NEX6-M	4159	3450	2050	2750	-91	4
				2750	3250	-42	12
				3250	4250	0	1
	NEX6-C	4159	3450	2050	2750	-89	11
				2750	3250	-37	12
				3250	4250	0	0
	LOCA5	4087	-	2050	3250	-59	5
				3250	4250	-13	1
	BCSD5	3903	4150	2050	3950	-43	4
	MACA5	4087	-	2050	3450	-59	5
				3450	4150	-13	1
	DBCCA6	4030	-	2050	2950	-94	2
				2950	4050	-65	4

References

Arsenault, K.R., Kumar, S.V., Geiger, J.V., Wang, S., Kemp, E., Mocko, D.M., Beaudoing, H.K., Getirana, A., Navari, M., Li, B., Jacob, J., Wegiel, J., Peters-Lidard, C.D., 2018. The Land surface Data Toolkit (LDT v7.2) – a data fusion environment for land data assimilation systems. Geoscientific Model Development 11, 3605–3621. https://doi.org/10.5194/gmd-11-3605-2018

Barlage, M., Zeng, X., Wei, H., Mitchell, K.E., 2005. A global 0.05° maximum albedo dataset of snow-covered land based on MODIS observations. Geophysical Research Letters 32. https://doi.org/10.1029/2005GL022881

Barsugli, J.J., Ray, A.J., Livneh, B., Dewes, C.F., Heldmyer, A., Rangwala, I., Guinotte, J.M., Torbit, S., 2020. Projections of Mountain Snowpack Loss for Wolverine Denning Elevations in the Rocky Mountains. Earth’s Future 8, e2020EF001537. https://doi.org/10.1029/2020EF001537

Batjes, N.H., 1995. A homogenized soil data file for global environmental research: A subset of FAO, ISRIC and NRCS profiles (Version 1.0). ISRIC.

Chiverton, A., Hannaford, J., Holman, I.P., Corstanje, R., Prudhomme, C., Hess, T.M., Bloomfield, J.P., 2015. Using variograms to detect and attribute hydrological change. Hydrology and Earth System Sciences 19, 2395–2408. https://doi.org/10.5194/hess-19-2395-2015

Cho, E., Vuyovich, C.M., Kumar, S.V., Wrzesien, M.L., Kim, R.S., Jacobs, J.M., 2022. Precipitation biases and snow physics limitations drive the uncertainties in macroscale modeled snow water equivalent. Hydrology and Earth System Sciences 26, 5721–5735. https://doi.org/10.5194/hess-26-5721-2022

Cosgrove, B.A., Lohmann, D., Mitchell, K.E., Houser, P.R., Wood, E.F., Schaake, J.C., Robock, A., Marshall, C., Sheffield, J., Duan, Q., Luo, L., Higgins, R.W., Pinker, R.T., Tarpley, J.D., Meng, J., 2003. Real-time and retrospective forcing in the North American Land Data Assimilation System (NLDAS) project. Journal of Geophysical Research: Atmospheres 108. https://doi.org/10.1029/2002JD003118

Daly, C., Halbleib, M., Smith, J.I., Gibson, W.P., Doggett, M.K., Taylor, G.H., Curtis, J., Pasteris, P.P., 2008. Physiographically sensitive mapping of climatological temperature and precipitation across the conterminous United States. International Journal of Climatology 28, 2031–2064. https://doi.org/10.1002/joc.1688

Daly, C., Taylor, G., Gibson, W., 1997. The PRISM approach to mapping precipitation and temperature, in: 10th Conference on Applied Climatology, American Meteorological Society, 20-23 October, Reno NV. pp. 10–12.

Eyring, V., Bony, S., Meehl, G.A., Senior, C.A., Stevens, B., Stouffer, R.J., Taylor, K.E., 2016. Overview of the Coupled Model Intercomparison Project Phase 6 (CMIP6) experimental design and organization. Geoscientific Model Development 9, 1937–1958. https://doi.org/10.5194/gmd-9-1937-2016

Fang, Y., Liu, Y., Margulis, S.A., 2020. A New Landsat-era Snow Reanalysis Dataset over the Western United States 2020, C047-0017.

Friedl, M.A., McIver, D.K., Hodges, J.C.F., Zhang, X.Y., Muchoney, D., Strahler, A.H., Woodcock, C.E., Gopal, S., Schneider, A., Cooper, A., Baccini, A., Gao, F., Schaaf, C., 2002. Global land cover mapping from MODIS: algorithms and early results. Remote Sensing of Environment, The Moderate Resolution Imaging Spectroradiometer (MODIS): a new generation of Land Surface Monitoring 83, 287–302. https://doi.org/10.1016/S0034-4257(02)00078-0

Friedl, M.A., Woodcock, C.E., Olofsson, P., Zhu, Z., Loveland, T., Stanimirova, R., Arevalo, P., Bullock, E., Hu, K.-T., Zhang, Y., Turlej, K., Tarrio, K., McAvoy, K., Gorelick, N., Wang, J.A., Barber, C.P., Souza, C., 2022. Medium Spatial Resolution Mapping of Global Land Cover and Land Cover Change Across Multiple Decades From Landsat. Frontiers in Remote Sensing 3.

Gelaro, R., McCarty, W., Suárez, M.J., Todling, R., Molod, A., Takacs, L., Randles, C.A., Darmenov, A., Bosilovich, M.G., Reichle, R., Wargan, K., Coy, L., Cullather, R., Draper, C., Akella, S., Buchard, V., Conaty, A., Silva, A.M. da, Gu, W., Kim, G.-K., Koster, R., Lucchesi, R., Merkova, D., Nielsen, J.E., Partyka, G., Pawson, S., Putman, W., Rienecker, M., Schubert, S.D., Sienkiewicz, M., Zhao, B., 2017. The Modern-Era Retrospective Analysis for Research and Applications, Version 2 (MERRA-2). Journal of Climate 30, 5419–5454. https://doi.org/10.1175/JCLI-D-16-0758.1

Günther, D., Marke, T., Essery, R., Strasser, U., 2019. Uncertainties in Snowpack Simulations—Assessing the Impact of Model Structure, Parameter Choice, and Forcing Data Error on Point-Scale Energy Balance Snow Model Performance. Water Resources Research 55, 2779–2800. https://doi.org/10.1029/2018WR023403

Jordan, R., 1991. A One-Dimensional Temperature Model for a Snow Cover: Technical Documentation for SNTHERM.89. (No. CRREL-SR-91-16). Cold Regions Research and Engineering Lab, Hanover, NH.

Kim, R.S., Kumar, S., Vuyovich, C., Houser, P., Lundquist, J., Mudryk, L., Durand, M., Barros, A., Kim, E.J., Forman, B.A., Gutmann, E.D., Wrzesien, M.L., Garnaud, C., Sandells, M., Marshall, H.-P., Cristea, N., Pflug, J.M., Johnston, J., Cao, Y., Mocko, D., Wang, S., 2021. Snow Ensemble Uncertainty Project (SEUP): quantification of snow water equivalent uncertainty across North America via ensemble land surface modeling. The Cryosphere 15, 771–791. https://doi.org/10.5194/tc-15-771-2021

Kumar, S.V., Peters-Lidard, C.D., Tian, Y., Houser, P.R., Geiger, J., Olden, S., Lighty, L., Eastman, J.L., Doty, B., Dirmeyer, P., Adams, J., Mitchell, K., Wood, E.F., Sheffield, J., 2006. Land information system: An interoperable framework for high resolution land surface modeling. Environmental Modelling & Software 21, 1402–1415. https://doi.org/10.1016/j.envsoft.2005.07.004

Livneh, B., Deems, J.S., Schneider, D., Barsugli, J.J., Molotch, N.P., 2014. Filling in the gaps: Inferring spatially distributed precipitation from gauge observations over complex terrain. Water Resources Research 50, 8589–8610. https://doi.org/10.1002/2014WR015442

Mahony, C.R., Wang, T., Hamann, A., Cannon, A.J., 2022. A global climate model ensemble for downscaled monthly climate normals over North America. International Journal of Climatology 42, 5871–5891. https://doi.org/10.1002/joc.7566

Margulis, S.A., Cortés, G., Girotto, M., Durand, M., 2016. A Landsat-Era Sierra Nevada Snow Reanalysis (1985–2015). J. Hydrometeor. 17, 1203–1221. https://doi.org/10.1175/JHM-D-15-0177.1

Niu, G., Yang, Z., Mitchell, K.E., Chen, F., Ek, M.B., Barlage, M., Kumar, A., Manning, K., Niyogi, D., Rosero, E., Tewari, M., Xia, Y., 2011. The community Noah land surface model with multiparameterization options (Noah-MP): 1. Model description and evaluation with local-scale measurements. Journal of Geophysical Research: Atmospheres 116. https://doi.org/10.1029/2010JD015139

Pflug, J., Margulis, S., Lundquist, J., 2021. Inferring Watershed-scale Mean Snow Magnitude and Distribution Using Multidecadal Snow Reanalysis Patterns and Snow Pillow Observations (preprint). Preprints. https://doi.org/10.22541/au.163250588.84772578/v1

Planton, S., Lionello, P., Artale, V., Aznar, R., Carrillo, A., Colin, J., Congedi, L., Dubois, C., Elizalde, A., Gualdi, S., 2012. The climate of the Mediterranean region in future climate projections. The Climate of the Mediterranean Region 449–502.

Raleigh, M.S., Lundquist, J.D., Clark, M.P., 2015. Exploring the impact of forcing error characteristics on physically based snow simulations within a global sensitivity analysis framework. Hydrol. Earth Syst. Sci. 19, 3153–3179. https://doi.org/10.5194/hess-19-3153-2015

Reifen, C., Toumi, R., 2009. Climate projections: Past performance no guarantee of future skill? Geophysical Research Letters 36. https://doi.org/10.1029/2009GL038082

Sheffield, J., Goteti, G., Wood, E.F., 2006. Development of a 50-Year High-Resolution Global Dataset of Meteorological Forcings for Land Surface Modeling. Journal of Climate 19, 3088–3111. https://doi.org/10.1175/JCLI3790.1

Sofaer, H.R., Barsugli, J.J., Jarnevich, C.S., Abatzoglou, J.T., Talbert, M.K., Miller, B.W., Morisette, J.T., 2017. Designing ecological climate change impact assessments to reflect key climatic drivers. Global Change Biology 23, 2537–2553. https://doi.org/10.1111/gcb.13653

Subyani, A.M., 2019. Climate variability in space-time variogram models of annual rainfall in arid regions. Arab J Geosci 12, 650. https://doi.org/10.1007/s12517-019-4836-8

Thrasher, B., Wang, W., Michaelis, A., Melton, F., Lee, T., Nemani, R., 2022. NASA Global Daily Downscaled Projections, CMIP6. Sci Data 9, 262. https://doi.org/10.1038/s41597-022-01393-4

Verseghy, D.L., 1991. Class—A Canadian land surface scheme for GCMS. I. Soil model. International Journal of Climatology 11, 111–133. https://doi.org/10.1002/joc.3370110202

Vögeli, C., Lehning, M., Wever, N., Bavay, M., 2016. Scaling Precipitation Input to Spatially Distributed Hydrological Models by Measured Snow Distribution. Front. Earth Sci. 4. https://doi.org/10.3389/feart.2016.00108

Wayand, N.E., Hamlet, A.F., Hughes, M., Feld, S.I., Lundquist, J.D., 2013. Intercomparison of Meteorological Forcing Data from Empirical and Mesoscale Model Sources in the North Fork American River Basin in Northern Sierra Nevada, California. Journal of Hydrometeorology 14, 677–699. https://doi.org/10.1175/JHM-D-12-0102.1

Wood, A.W., Leung, L.R., Sridhar, V., Lettenmaier, D.P., 2004. Hydrologic Implications of Dynamical and Statistical Approaches to Downscaling Climate Model Outputs. Climatic Change 62, 189–216. https://doi.org/10.1023/B:CLIM.0000013685.99609.9e

Wrzesien, M.L., Kumar, S., Vuyovich, C., Gutmann, E.D., Kim, R.S., Forman, B.A., Durand, M., Raleigh, M.S., Webb, R., Houser, P., 2022. Development of a “Nature Run” for Observing System Simulation Experiments (OSSEs) for Snow Mission Development. Journal of Hydrometeorology 23, 351–375. https://doi.org/10.1175/JHM-D-21-0071.1